Towards an engineering tool for the prediction of running ductile fractures in CO_2 pipelines

Hans Langva Skarsvåg[a], Morten Hammer[a], Svend Tollak Munkejord[a,*], Alexandra Metallinou Log[c], Stéphane Dumoulin[b], Gaute Gruben[b]

[a] *SINTEF Energy Research, P.O. Box 4761 Torgarden, NO-7465 Trondheim, Norway*
[b] *SINTEF Industry, P.O. Box 4760 Torgarden, NO-7465 Trondheim, Norway*
[c] *Norwegian University of Science and Technology, Department of Energy and Process Engineering, NO-7491 Trondheim, Norway*

Abstract

A prerequisite for the deployment of CO_2 capture and storage (CCS) is to establish a large network of high-pressure transport pipelines. It is then vital to assess new and existing pipeline designs for running ductile fracture (RDF). RDF is a phenomenon in which a defect develops into a crack propagating along the pipeline, sustained by the pressure forces from the escaping fluid. The most common engineering method for RDF, the Battelle two-curve method (BTCM), was originally developed for natural gas (NG) and has proved non-conservative for CO_2.

In this work we examine the BTCM in the light of available RDF experiments with CO_2-rich mixtures. We present an improved material curve, in which the change in fluid properties when replacing NG with CO_2 results in a new effective toughness correlation. Furthermore, we present an improved method for calculating the crack-tip pressure. This delayed homogeneous equilibrium model (D-HEM) accounts for the non-equilibrium thermodynamics due to the rapid depressurization, resulting in boiling pressures below the saturation pressure. Together, the adaptation of the material and fluid treatment yields improved results, and is a step towards a viable engineering tool for the prediction of RDF in CO_2 pipelines.

Keywords: CO_2 pipelines, running ductile fracture, carbon dioxide, decompression, non-equilibrium, pipeline integrity

1. Introduction

CO_2 capture and storage (CCS) is regarded as one of the technologies needed in order to mitigate climate change (Edenhofer *et al.*, 2014). In the IEA (2021) scenario to reach net zero emissions by 2050, 7.6 gigatonnes of CO_2 are captured globally per year, out of which 95 % is permanently stored. By mass, this is more than the global production of natural gas (NG), which was about 4000 billion standard cubic metres in 2020 (IEA, 2021), corresponding to about 2.8 gigatonnes.

Because capture plants and storage sites are in general not colocated, a large-scale CO_2-transportation system needs to be deployed, including pipelines and ships. Due to the sheer size of the system, optimized and safe design and operation will be crucial, taking the properties of CO_2 and CO_2-rich mixtures into account (Bilio *et al.*, 2009; d'Amore *et al.*, 2018; Gu *et al.*, 2018, 2019; Martynov *et al.*, 2014; Munkejord *et al.*, 2016; Vitali *et al.*, 2022; Zhao and Li, 2014). The impurities present in CO_2 streams can roughly be divided into two categories, (i) 'non-condensable gases' such as N_2, Ar, H_2 and CH_4, which can be present in the range of percent, and which can therefore significantly affect the

*Corresponding author.
Email address: svend.t.munkejord [a] sintef.no (Svend Tollak Munkejord)

thermophysical properties (Munkejord *et al.*, 2016), and (ii) potentially reactive impurities such as NOx and SOx, which must be limited to the ppmv range in order to avoid corrosion in carbon steel pipelines (Morland *et al.*, 2022).

The deployment of CO_2 pipelines requires safety assessments, including, among other things, the dispersion of CO_2 in the terrain in the event of an accidental release. Such a release could be caused by equipment failure, corrosion, maintenance errors, external impacts and operator errors (Pham and Rusli, 2016). With the aim of estimating safety distances to CO_2 transportation pipelines, quantitative risk assessments (QRA) have been proposed (Teng *et al.*, 2021).

In order to limit the consequences of a failure or rupture, pipelines transporting highly pressurized compressible fluids need to be designed to avoid running ductile fracture (RDF) for more than 1–2 pipe sections (DNV, 2012). RDF is a phenomenon whereby a defect in the pipeline, caused by e.g. corrosion or accidental loads, develops into a fracture running along the pipe, sustained by the pressure forces from the escaping fluid. The most commonly used design method to assess RDF, the Battelle two-curve method (BTCM) (Maxey, 1974) is semi-empirical and was developed for NG pipelines in the 1970s. It relies on the assumption that the crack-propagation speed in the steel and the decompression-wave speed in the fluid are independent. These quantities are drawn as a function of pressure level (hence the name, see Figure 1) and the resulting method has had considerable practical impact. A major difference between CO_2 and NG during RDF is that for typical conditions, CO_2 boils while NG does not. Therefore, the fluid curve for CO_2 in Figure 1a has a plateau as opposed to the curve for NG in Figure 1b.

The BTCM gives a good indication of the arrest/propagation boundary for steel pipes with yield strength less than 450 MPa and Charpy V-notch values (C_{VN}) less than 100 J. However, most modern steels have C_{VN} values larger than 150 J, and it has been demonstrated that the original BTCM had to be modified to capture the arrest/propagate boundary for such steels (Leis *et al.*, 1998; Wilkowski *et al.*, 1977). Recent studies have shown that these toughness-modified versions of the BTCM do not provide conservative results for CO_2 pipelines (Cosham *et al.*, 2012, 2014), presumably since they do not include enough relevant physics (Aursand *et al.*, 2016a).

Maxey (1986) addressed the differences between NG pipelines and CO_2 pipelines with respect to RDF. He proposed that fracture arrest will occur if the CO_2 boiling pressure is lower than the pipe's 'arrest pressure' which is a function of pipe geometry and material properties. This approach is mentioned in ISO (2016) where a safety factor for the calculated arrest pressure is recommended for cases where C_{VN} is less than 330 J.

Michal *et al.* (2020) and DNVGL (2021) proposed a modification of the BTCM based on available full-scale fracture arrest tests for CO_2. It defines a region of likely propagation, a region of likely arrest, and a transition region between these two, where the boundary resides. In DNVGL (2021), a relatively large area is labelled 'evaluation based on assessments'. This indicates the scarcity of experiments for certain pipe configurations. In addition, for some conditions, an increase of the pipe-wall thickness could lead to a more strict evaluation.

Recently, efforts have been made to develop coupled fluid-structure models that can predict RDF in CO_2 pipelines (Aursand *et al.*, 2016a; Gruben *et al.*, 2019; Keim *et al.*, 2019, 2020; Nakai *et al.*, 2016; Nordhagen *et al.*, 2017; Talemi *et al.*, 2019). While there is good reason to believe that such models can incorporate more physics and therefore help providing better predictions, they remain highly specialized tools requiring long computational times.

For practical engineering purposes, therefore, there is a need to develop a tool of similar ease of use as the Battelle two-curve method, and with increased predictive capability for CO_2 pipelines. Our hypothesis is that this is possible, by drawing more appropriate fluid and material curves. Furthermore, it should be possible to do this by taking more of the governing physics into account, rather than using purely empirical correlations. Thus, the aim of the current work is to improve both the material and fluid curves.

(i) Material curve: The original Battelle two-curve method was developed for NG, assuming that the crack-tip pressure alone sufficiently describes the forces acting on the pipe. However, for liquid or dense-phase operating conditions, CO_2 will boil during depressurization, leading to a different pressure

distribution, especially behind the crack-tip on the flaps, see e.g. Aursand *et al.* (2016a). It is likely that this would lead to a different functional form of the material curve.

(ii) Fluid curve: When employing the BTCM for CO_2 pipelines, it is customary to assume that the crack-tip pressure is equal to the gas-liquid equilibrium pressure calculated by an isentropic expansion from the operational state (Cosham *et al.*, 2012; Gu *et al.*, 2018). However, the importance of considering non-equilibrium for CO_2 expansion was emphasized by Benintendi (2014). Lopes *et al.* (2018) presented an outflow model taking non-equilibrium into account, but did not discuss the resulting pressure level. It has been experimentally observed during crack-propagation tests that the pressure is lower than that predicted assuming equilibrium (Cosham *et al.*, 2012; Michal *et al.*, 2020). It is reasonable to assume that thermodynamic equilibrium does not have time to establish itself during the few milliseconds the depressurization process lasts, and this will affect the observed pressure levels (Flechas *et al.*, 2020). Furthermore, the degree of pressure 'undershoot' with respect to the equilibrium value is dependent on the initial state, see Munkejord *et al.* (2020). It should also be noted that an accurate equation of state (EoS) is of primary importance in order to obtain an accurate fluid curve. See, e.g., the discussion of the effect of density and speed of sound in Munkejord *et al.* (2021).

In the present work, we investigate both of the above topics. First, we modify the material curve by changing the arrest-pressure functional form. Next, we modify the fluid curve by employing the recent 'delayed homogeneous equilibrium model' (D-HEM) (Hammer *et al.*, 2022) taking non-equilibrium into account. While the resulting model is not intended to be the 'final' answer, and further work is needed, we show that the present approach holds significant promise, by comparing with experimental data (Cosham *et al.*, 2016) and obtaining significantly better match than with the original two-curve method. Finally, the present approach is relatively easy to implement as an engineering tool that can be used by pipeline engineers – not requiring specialists within finite-element methods (FEM) or computational fluid dynamics (CFD) in order to provide predictions.

The rest of this paper is organized as follows. Section 2 introduces and briefly discusses the BTCM. In Section 3, we present a modified two-curve method and evaluate it using full-scale fracture propagation test data. Section 4 concludes the work.

2. The Battelle two-curve method

This section briefly discusses the Battelle two-curve method (BTCM) in the context of CO_2 pipelines. The acceleration or deceleration of a running ductile fracture (RDF) is dependent on the balance between energy dissipation and the work done by high-pressure fluid that is exposed as the crack propagates. The driving force, determined by the pressure profile in the vicinity of the crack tip, will be lowered if the decompression-wave speed is faster than the crack-tip velocity. In the opposite case, if the crack-tip velocity is faster than the decompression-wave speed, the pressure-determined driving force will increase. Steady-state propagation occurs when these two velocities are equal, see Figure 1. If the crack-tip velocity as a function of the crack-tip pressure, $v_{ct}(P_{ct})$ (material curve), and the decompression-wave speed as a function of fluid properties (fluid curve) are known, one can analyse the evolution from fracture initiation. The fluid and material curves are the *two curves* of the BTCM. An intersection of these two curves indicates that a steady state will form provided that the initial fluid pressure inside the pipe is higher than the pressure at the intersection. Figure 1b illustrates the BTCM for three scenarios, (i) arrest, (ii) slow arrest, (iii) propagate, with a fluid curve resembling that of (dry) NG. In the following, we will present the fluid curve for CO_2 and the material curve as illustrated in Figure 1a, and how the latter can be influenced by the fluid dynamics.

2.1. Material curve

The material curve correlates the fluid pressure at the crack tip to the crack-tip velocity, $P_{ct}(v_{ct})$. From full-scale fracture-propagation tests with NG, this relation has empirically been found to be (Maxey, 1974)

$$P_{ct} = P_a \left[1 + \left(v_{ct} \frac{\sqrt{C_{VN}/A}}{K_{BF}\bar{\sigma}} \right)^6 \right], \tag{1}$$

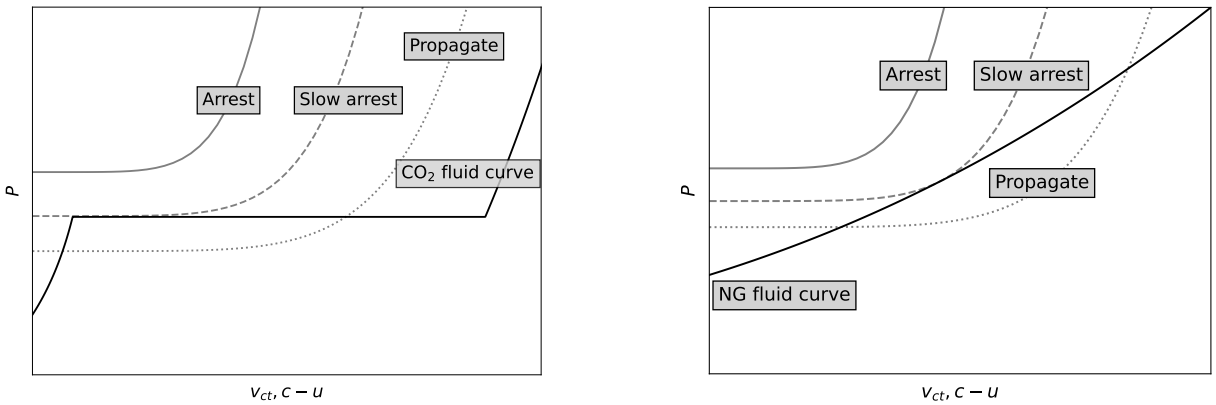

(a) BTCM for CO_2.

(b) BTCM for (dry) NG.

Figure 1: Illustration of the Battelle two-curve method (BTCM) for CO_2 and (dry) natural gas (NG) showing an example fluid curve and material curves that would result in propagating and arresting fractures, as well as the limiting case of slow arrest.

where C_{VN}/A is the Charpy V-notch value divided by the Charpy specimen cross-section, K_{BF} is a parameter that accounts for the backfill, and the flow stress, $\bar{\sigma}$, is found from the yield stress, σ_{ys}, as $\bar{\sigma} \equiv \sigma_{ys} + 68.95\,\text{MPa}$. The arrest pressure, P_a, is the threshold pressure, below which a crack will not propagate. According to the strip-yield model (Kiefner *et al.*, 1973) it is

$$P_a = \frac{2\bar{\sigma}t}{M_T \pi R} \arccos\left[\exp\left(-\frac{K_{mat}^2 \pi}{8 a_c \bar{\sigma}^2}\right)\right]. \tag{2}$$

Here t, is the pipe thickness, R is the radius and $M_T(a_c/\sqrt{Rt})$ is the Folias function which accounts for stress amplification at the crack tip in pressurized pipes, resulting from the outward radial deflection along the crack (Folias, 1970):

$$M_T = \left(1 + 1.255\frac{a_c^2}{Rt} - 0.0135\frac{a_c^4}{R^2 t^2}\right)^{1/2}, \tag{3}$$

where a_c is the half-length of the through-wall flaw. For a propagating crack, a_c must be replaced by an effective value empirically found to be $a_c^{\text{eff}} = 3\sqrt{Rt}$, which then yields $M_T \approx 3.33$. The material toughness parameter K_{mat} is a material dependent parameter related to the material's resistance to fracture (Maxey *et al.*, 1972).

The material toughness is usually inferred from small-scale tests. It has been found that there is a 1:1 relation between the Charpy V-notch value and the material toughness squared

$$K_{mat}^2 = E\frac{C_{VN}}{A}, \tag{4}$$

where E is the Young's modulus of the material. This relation has been developed by correlating full-scale burst data to small-scale experiments (Maxey *et al.*, 1972).

A capability to acquire the relevant material parameters to a sufficient accuracy, without the need for full-scale tests, is essential for the usefulness of the BTCM. Since the BTCM was developed for NG pipelines, the correlations and effective parameters have been verified by and correlated from NG pipeline experiments. The material curve is set up to correlate the pressure at the crack tip to the crack-tip velocity. Because the fluid properties influence the pressure and hence force distribution, it appears reasonable that they have an impact on this correlation. That is, it is unlikely that two identical

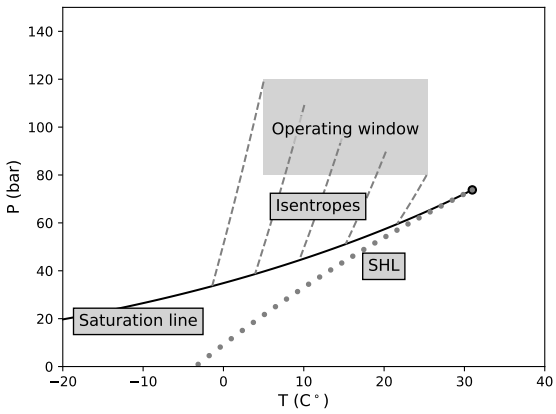

Figure 2: Illustration of typical operating window and decompression paths (isentropes) in a temperature–pressure phase diagram.

pipes carrying NG and CO_2 will have the same steady-state crack-tip velocity, v_{ct}, at the same crack-tip pressure, P_{ct} (P_{ct} can in theory be adjusted by tuning the initial pressure and temperature). A more sophisticated model could include calculations of the pressure profile, and correlate the velocity to the pressure decay function. Because of the simplicity required to make a useful engineering tool, we here keep the method of pressure-point-value correlation of the original BTCM. The effect of a changed pressure profile due to different fluid properties when replacing NG with CO_2 must therefore be captured by other parameters, such as the toughness correlation given by Eq. (4) or a_c^{eff}.

2.2. Fluid curve for CO_2

The typical operating pressure of a CO_2 pipeline is well above the critical pressure ($P_{cr} = 73.8$ bar). The CO_2 is thus in a liquid-like state. Rapid decompression is close to isentropic, and follows the isentrope into the two-phase region, where CO_2 starts boiling. Figure 2 illustrates decompression curves originating in a typical pipeline operating window and hitting the gas-liquid two-phase saturation line (for pure CO_2). One can observe that, perhaps counter-intuitively, a higher operating pressure leads to a lower saturation pressure upon decompression.

The phase change observed for CO_2 is in contrast to the case for dry NG, which follows the relevant isentrope through the gas region. The liquid-to-gas phase change is associated with significant volume increase and a larger amount of available work. This can be demonstrated by calculating the pressure (force) and available work ($\int p\,\mathrm{d}V$) along two isentropes for CO_2 and pure methane. In Figure 3 this has been done for the isentropes that correspond to a crack-tip pressure of $P_{ct} = 70$ bar. The qualitative picture does not change by changing the reference pressure, and 70 bar is chosen because it is close to the worst-case scenario where P_{ct} is at critical pressure of CO_2. By plotting pressure as a function of the change in relative volume, we get an indication of how the pressure is reduced behind the crack tip, see Figure 3a. For methane, a 50 % reduction in pressure occurs at 65 % volume increase, while for CO_2, the same pressure reduction occurs at approximately three times that volume increase (180 %). This results in a significantly larger available work for CO_2, e.g., 60 % larger available work for a 300 % volume increase, see Figure 3b. The estimated pressure decay is also in line with full-scale experimental results for NG (Ives *et al.*, 1974) and CO_2 (Aursand *et al.*, 2016a).

The decompression-wave speed, $c - u$, is determined by the speed of sound of the rarefaction wave, c, relative to the flow velocity, u. This speed is found by analysis of the Euler equations, assuming one-dimensional isentropic quasi-steady flow. The result is

$$c(P) - |\mathbf{u}(P)| = c(P) - \int_P^{P_0} \frac{\mathrm{d}P'}{\rho(P')c(P')}, \tag{5}$$

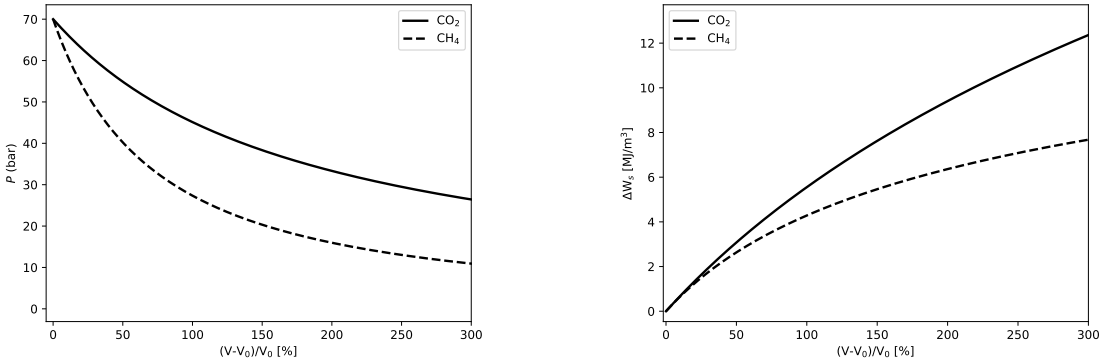

(a) Pressure along isentropes vs relative volume change. (b) Available work along isentropes vs relative volume change.

Figure 3: A comparison of the pressure and available work for methane and pure CO_2 along the isentropes corresponding to a crack-tip pressure of 70 bar. The volume is normalized by the initial volume, V_0.

where ρ is the fluid density and P_0 is the initial pressure. When deriving the above expression, full thermodynamic equilibrium is assumed, i.e., for a two-phase state, the phases have the same pressure, temperature and chemical potential. This assumption leads to a discontinuous speed of sound at the phase boundary, see Linga and Flåtten (2019), and further, to a jump in the decompression-wave speed as a function of pressure. This has significant implications for the BTCM, since it creates a plateau in the fluid curve in the region where one would expect intersection of the two curves. Typically the plateau pressure will be in the range from 40 bar up to the maximum two-phase pressure, which can be more than 80 bar for CO_2-rich mixtures, see Section 3.2.

When the decompression process is rapid, the nucleation of vapour bubbles is too slow to keep the fluid in thermodynamic equilibrium. In crack-propagation experiments, the plateau pressure has therefore been observed to be lower than the saturation pressure (Cosham *et al.*, 2012; Michal *et al.*, 2020). Munkejord *et al.* (2020) observed that for tube-depressurization experiments, the experimentally recorded plateau pressure lay between that calculated assuming equilibrium and that calculated with no phase transfer. Analysis with the crack-tip pressure as input therefore requires a non-equilibrium thermodynamic model for the estimation of the pressure. One such model is presented in Sec. 3.2.

3. Improved model for predicting running ductile fractures in CO_2 transportation pipelines

This section describes an approach to obtain improved RDF predictions for CO_2 pipelines using the BTCM framework. We first consider the material curve, next the fluid curve, and then we illustrate the performance of the model by applying it to experimental data from COOLTRANS Tests 1 and 2.

3.1. Crack-tip propagation model adapted to running ductile fracture experimental results

Several experiments on RDF in CO_2 pipelines have been conducted (Aursand *et al.*, 2016a; Cosham *et al.*, 2014, 2016; Di Biagio *et al.*, 2017; Michal *et al.*, 2018), see Table 1. The data from these experiments have been extracted and listed by Michal *et al.* (2020). Based on these data, Michal *et al.* mapped values of the arrest-curve parameters to the regions of expected arrest

$$\begin{aligned} R_\mathrm{f} &\geq 3.1, \\ R_\sigma &\leq 0.0208 R_\mathrm{f} + 0.1696, \\ R_\sigma &\leq 0.2739. \end{aligned} \tag{6}$$

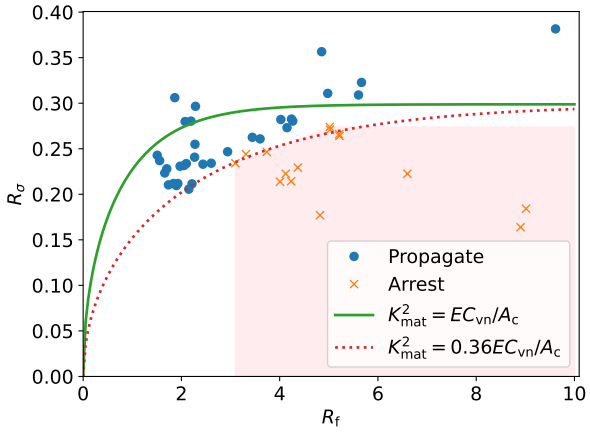

Figure 4: Experimental data on CO_2 RDF and arrest curves. The arrest curve in Eq. (2) with both the conventional toughness correlation (green) and adapted correlation (red dashed) is included. The shaded pink region denotes expected arrest according to Eq. (6).

Herein,

$$R_f = \frac{\pi C_{VN} E}{24 A \bar{\sigma}^2 \sqrt{Rt}} \tag{7}$$

is the fracture resistance parameter, and

$$R_\sigma = \frac{P_{ct} R}{t \bar{\sigma}} \tag{8}$$

is the stress-ratio parameter. Note that there is an additional factor 1000 appearing in R_f in Michal *et al.* (2020) because the units MPa and mm are used instead of SI units, and slightly different coefficients since they employed gauge pressure (MPag). The sparse experimental data makes the region of uncertain propagate/arrest quite large.

We now revisit the crack-arrest parameters appearing in Eq. (2). We hypothesize that because of the difference in forces acting at the crack tip when NG is replaced by CO_2, parameters such as the effective crack length, a_c^{eff}, flow stress or material toughness parameter should be scaled. The steel properties themselves are not altered, but the apparent properties appearing in the simplified correlation in Eq. (2) could be different due to the different fluid-structure interaction when NG has been replaced by CO_2. Using the toughness parameter K_{mat} in the tuning is the simplest way of getting a good fit to the data. Inserting

$$K^2_{\text{mat,eff}} = 0.36 E C_{VN} / A \tag{9}$$

in Eq. (2) gives a reasonable fit. The result is shown in Figure 4, where we have also shaded the safe region defined by Eq. (6). We believe that this new curve can be a useful step in adapting the BTCM to CO_2. This also emphasizes the need for more experiments, both in the flow-stress-dependent region (high R_f), where the curve reaches a plateau, and far into the toughness-dependent region ($R_f < 3$). In both of these regions the lack of data imply a large degree of uncertainty (Michal *et al.*, 2018). In these regions, the material curve, Eq. (2), will be correct only to the extent that the relevant physics are captured.

Cosham *et al.* (2022) recently modified the material curve by tuning the empirical relation between the effective crack length, a_c^{eff}, and $\sqrt{Rt}$. It should be noted that employing the toughness parameter, K_{mat}, is different, because a_c^{eff} also appears implicitly in the prefactor of the arccos function in Eq. (1) through the Folias factor in Eq. (3). We found that Eq. (9) gave the best result, reducing the need for conservatism. Some interesting observations can be made from this adaptation of the BTCM. Firstly, the toughness-dependent region, where the arrest behaviour depends on C_{VN}, becomes much larger

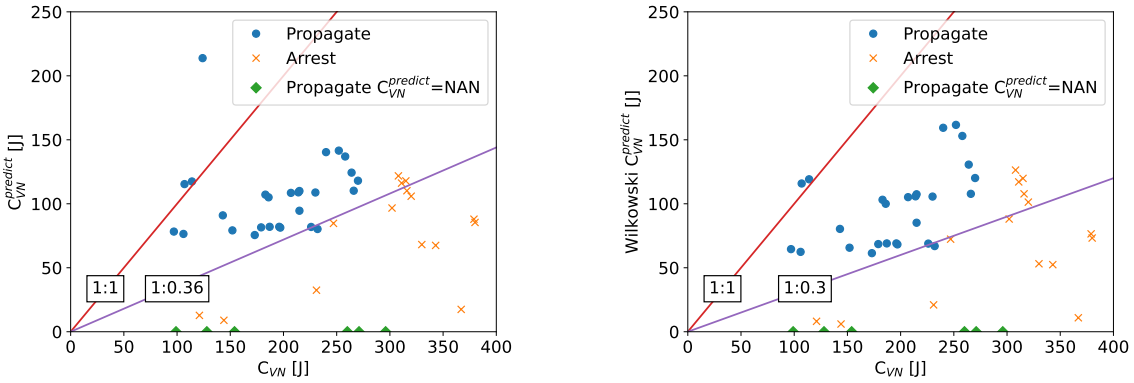

(a) Actual and predicted C_{VN} (without Wilkowski correction). (b) Actual and predicted C_{VN} with Wilkowski correction, Eq. (10).

Figure 5: Actual versus predicted Charpy V-notch values with and without the Wilkowski correction predicted by the BTCM. C_{VN} NAN indicates that the crack will propagate for arbitrarily high C_{VN}.

(dashed red curve in the figure) as it is a straight vertical line ($R_f = 3.1$) in the approach suggested by Michal *et al.* (2020). The implication for design is that an increase in steel toughness still pays off for relatively high-toughness steel. Secondly, a reasonably good fit could be made without special treatment of high-toughness steels such as the Wilkowski correction of the C_{VN} used for NG-carrying pipelines (Wilkowski *et al.*, 2000):

$$C_{VN}^{W} = 0.043(0.102C_{VN} + 10.29)^{2.597} - 16.81 \text{ for B to X70 steel.} \tag{10}$$

This becomes even more apparent when plotting the actual C_{VN} versus the C_{VN} predicted from Eq. (2), see Figure 5. Here, Eq. (2) has been solved for C_{VN} employing the standard toughness correlation in Eq. (4). One possible cause for this behaviour could be the fluid-pressure profile for CO_2, with a larger high-pressure region than for NG. It is also interesting to note that when the original BTCM was developed, only low-toughness steels ($C_{VN} \lesssim 100$ J) were used. When tougher steel types became available, moving the fracture dynamics into the flow-stress dominated regime, corrections had to made, such as the one by Wilkowski *et al.* (2000). For CO_2 it seems that the toughness-dominated regime is increased, and at the same time there is less need for a C_{VN}-dependent correction factor. That is, corrections such as the Wilkowski correction do not improve the results here.

3.2. Fluid decompression model taking non-equilibrium into account

Usually the calculation of the fluid decompression-wave speed in BTCM is conducted using the homogeneous equilibrium model (HEM). In HEM it is assumed that the phases, usually liquid (ℓ) and vapour (v), are in mechanical, chemical and thermal equilibrium. These assumptions lead to the pressure plateau in the fluid curve forming at the pressure where the liquid isentrope intersects the two-phase saturation curve, P_{sat}. However, full-scale RDF experiments (Aursand *et al.*, 2016a; Cosham *et al.*, 2014, 2016; Di Biagio *et al.*, 2017; Michal *et al.*, 2018) suggest that the observed pressure is generally lower than the saturation pressure. In addition, it has been observed that the pressure plateau is not really a plateau, but rather a slope. This is due to friction, heat transfer, pressure recovery due to phase transition, and possibly other factors, see Munkejord *et al.* (2020, Fig. 10). In the following, we will disregard the slope and concentrate on the pressure level.

3.2.1. Delayed nucleation

There are many complex phenomena in the fluid flow that may contribute to the reduced pressure level during RDF. However, obtaining a pressure-undershoot below the saturation pressure is a well-known phenomenon also for 'normal' full-bore pipe depressurizations, both for CO_2 and other fluids

(Barták, 1990; Borkar *et al.*, 1977; Botros *et al.*, 2016; Lienhard *et al.*, 1978; Munkejord *et al.*, 2020, 2021). This phenomenon is generally understood to be caused by delayed phase change, which is a non-equilibrium effect. The creation of gas bubbles requires energy, and the decompression is too fast for the energy to be supplied by the fluid's surroundings. Therefore, the phase change is delayed until the liquid has enough energy within itself to create bubbles through random thermal fluctuations (Debenedetti, 1997). This process is called nucleation. Before nucleation starts, the liquid is at a temperature above its boiling-point temperature and its state is denoted as 'superheated'.

The experimentally attainable limit of superheat, the largest superheat possible before phase change is observed, can be estimated using classical nucleation theory (CNT). CNT describes the homogeneous nucleation, which dominates at high temperatures. In contrast, heterogeneous nucleation occurs on a surface or impurity which lowers the energy barrier of bubble formation, and it therefore dominates at lower temperatures. Aursand *et al.* (2016b) found good agreement with experiments of the superheat limit (SHL) for pure CO_2 and the SHL obtained using CNT. Wilhelmsen and Aasen (2022) applied the SHL found using CNT to estimate choked CO_2 and water flows through nozzles by accounting for delayed phase change in the high-temperature range. It was found that heterogeneous nucleation started to dominate at a temperature of approximately 12 °C at the SHL for CO_2. The transition from one mode of nucleation to the other was observed to be gradual and the homogeneous nucleation model is therefore also expected to give reasonable results somewhat below $T = 12\,^{\circ}\mathrm{C}$. However, for a complete model description down to the triple point, a heterogeneous nucleation model is required, and this is left to future work.

3.2.2. Delayed homogeneous equilibrium model

Most models that account for delayed phase change require a full computational fluid dynamics (CFD) simulation. A simplified delayed homogeneous equilibrium model, D-HEM, avoiding detailed spatial and temporal resolution, was developed by Hammer *et al.* (2022). They applied D-HEM to pure CO_2 and steady-state flow in nozzles and orifices. In the present work, the D-HEM formalism has been applied to the rarefaction wave of the decompressing pipeline, and it has also been extended to fluid mixtures. The main difference between the pure fluid and mixture model lies in how the SHL is calculated, and this is detailed in Appendix B.1. In addition, Appendix B.2 quantifies the SHL sensitivity to two main parameters, namely, the critical nucleation rate and the surface tension.

It should be noted that CNT applied to mixtures is less accurate than when applied to pure fluids, especially for strongly interacting molecules (Aasen *et al.*, 2020). However, because the CO_2 mixtures considered in this work consist of relatively simple molecules without strong interactions, without self or cross association, we expect CNT to give reasonable results.

Figures 6 and 7 illustrate the fluid behaviour calculated using HEM and D-HEM for COOLTRANS Test 2. In Figure 6 we have plotted the phase diagram of the CO_2 mixture (see Table 2) including the saturation curve, the liquid SHL and the liquid limit of stability, also called the spinodal. The decompression paths calculated using HEM and D-HEM are the same, except at the important stage between the saturation curve and the SHL. This is highlighted in Figure 6b, showing the effect of the different steps of the D-HEM calculation. Figure 7 shows the pressure level plotted as a function of decompression-wave speed, to be employed in the BTCM. We observe that in this case, D-HEM yielded a plateau pressure 8 bar lower than HEM.

The following steps are taken when calculating the fluid decompression curve using D-HEM. The numbers refer to the process steps indicated in Figure 6b.

1. Beginning at the initial pressure of the pipe, integrate towards lower pressures using Eq. (5) with single-phase liquid properties at constant entropy.
2. Instead of assuming that nucleation begins at the pressure where the liquid isentrope crosses the bubble line, continue calculating the integral along the liquid isentrope until P_{SHL} is reached, i.e., where the isentrope crosses the liquid SHL. This accounts for the delayed nucleation of bubbles.
3. At the SHL, assume that all phase transfer occurs instantaneously from the SHL point to a two-phase equilibrium state denoted with the subscript eq. It is assumed that the phase change is

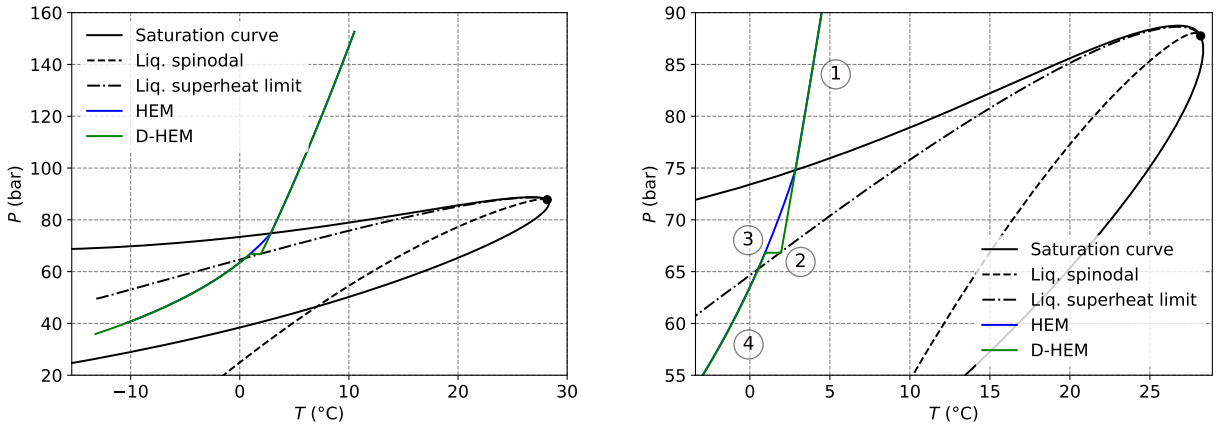

(a) Overview.

(b) The steps in the D-HEM calculation (zoom-in).

Figure 6: Fluid phase diagram for COOLTRANS Test 2 (Cosham *et al.*, 2016) with decompression path calculated using HEM and D-HEM.

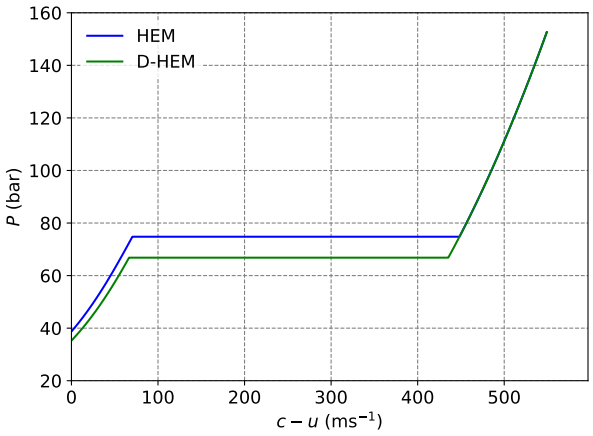

Figure 7: Fluid decompression curves in the BTCM method for COOLTRANS Test 2 (Cosham *et al.*, 2016) calculated using HEM and D-HEM.

isenthalpic and isobaric, and the fluid velocity stays constant, such that

$$P_{\mathrm{SHL}} = P_{\mathrm{eq}},\ h_{\mathrm{SHL}} = h_{\mathrm{eq}},\ u_{\mathrm{SHL}} = u_{\mathrm{eq}}. \tag{11}$$

With these assumptions, the instantaneous phase change provides a slight entropy production. This means that the model is in agreement with the second law of thermodynamics.

4. Continue calculating the fluid curve properties using Eq. (5) with HEM from P_{eq} until the choke pressure, P_{choke}, is reached when $c - u = 0$.

For the calculation of thermophysical properties, we employ our in-house framework (Hammer *et al.*, 2020; Wilhelmsen *et al.*, 2017) using the GERG2008 EoS (Kunz and Wagner, 2012). The development of the GERG-2008 EoS was purely based on experimental measurements of stable thermodynamic states. In addition, the EoS exhibits an additional unphysical Maxwell-loop in the unstable area. The accuracy in the metastable liquid region and the accuracy in predicting the spinodal curve is therefore unknown. Alternative EoSs based on statistical thermodynamics are expected to be more physically correct in

Table 1: Initial temperature (T_0) and pressure (P_0), and crack-tip pressure (P_{ct}) interpreted by Michal *et al.* (2020), for various fracture-propagation tests, and plateau pressure calculated using the HEM and D-HEM models, along with the deviation (ε) from the experimental value.

Test	T_0 (°C)	P_0 (bar)	P_{ct} (bar)	P_{HEM} (bar)	ε (%)	$P_{D\text{-}HEM}$ (bar)	ε (%)
CO2PIPETRANS 1 (Aursand *et al.*, 2016a)	30.0	89.5	54	63.7	18	61.6	14
CO2PIPETRANS 2 (Aursand *et al.*, 2016a)	8.6	92.5	26	38.5	48	12.1*	53*
COOLTRANS-1 (Cosham *et al.*, 2014, 2016)	13.1	150.3	73.5	81.0	10	77.1	5
COOLTRANS-2 (Cosham *et al.*, 2014, 2016)	10.5	152.6	66.4	74.8	13	66.8	1
COOLTRANS-3 (Cosham *et al.*, 2016)	15.0	152.2	82	90.0	10	88.0	7
SARCO2-B (Di Biagio *et al.*, 2017)	17.8	128.0	68	73	7	70.0	3
CO2SAFE-ARREST 1 (Michal *et al.*, 2018, 2020)	11.6	151.4	65	79.5	22	76.1	17
CO2SAFE-ARREST 2 (Michal *et al.*, 2020)	12.8	149.7	74.5	84.9	14	83.0	11

*T, P lower than the range of validity of D-HEM.

Table 2: CO_2 mixture composition (mole%) in fracture-propagation tests.

Test	CO_2	N_2	H_2	O_2	CH_4
CO2PIPETRANS 1	100.0	–	–	–	–
CO2PIPETRANS 2	100.0	–	–	–	–
COOLTRANS-1	90.9	4.0	1.0	1.8	2.2
COOLTRANS-2	93.7	3.4	1.1	1.8	–
COOLTRANS-3	90.3	6.6	1.1	2.0	–
SARCO2-B	94.0	6.0	–	–	–
CO2SAFE-ARREST 1	91.1	8.9	–	–	–
CO2SAFE-ARREST 2	89.8	10.2	–	–	–

the metastable region. However, the density and speed-of-sound prediction of the GERG-2008 EoS are far superior in the stable domain compared to alternative EoSs, and they are therefore used in this work. How far the better predictions will extend into the metastable region is unknown, but the use of a highly accurate EoS ensures that most of the deviation in the calculation of the thermodynamic properties will stem from the D-HEM approach. In the present work, the mixture surface tension is predicted using the parachor method applied in REFPROPv10 (Huber *et al.*, 2022). The accuracy of the the parachor method is discussed in Appendix A.

In Table 1, we compare plateau pressures calculated using HEM and D-HEM with the crack-tip pressure evaluated by Michal *et al.* (2020) for several relevant full-scale RDF experiments. For reference, the CO_2 mixture compositions are given in Table 2. It can be seen that the deviation between the experiments and calculations are significantly reduced for all experiments when employing D-HEM instead of HEM. One exception is CO2PIPETRANS Test 2. This result is expected, because the isentrope crosses the SHL at a temperature about 11 °C below the point where heterogeneous nucleation begins to dominate. As the SHL only accounts for homogeneous nucleation, D-HEM cannot provide a good estimate of the plateau pressure for this test. Furthermore, the pipes used in the CO2PIPETRANS tests were short, which could mean the propagating crack had not reached a steady state by the time the relevant sensor was reached. This is particularly true for Test 2, in which the fracture arrested after roughly 1 m.

3.3. Evaluation of the modified two-curve method applied to COOLTRANS Tests 1 and 2

We now evaluate our modified two-curve method by studying COOLTRANS Tests 1 and 2 (Cosham *et al.*, 2016) in more detail. These tests are chosen because they both produced several data points and the crack-tip pressure was high enough to make D-HEM applicable. In COOLTRANS Test 1, the fracture propagated from initiation at the centre of the pipe length, through three sections on the east side and four sections on the west side. The crack arrested in the last of these sections. With the initiation segments this gives a total of nine data points with the same initial conditions (see Table 1) for the

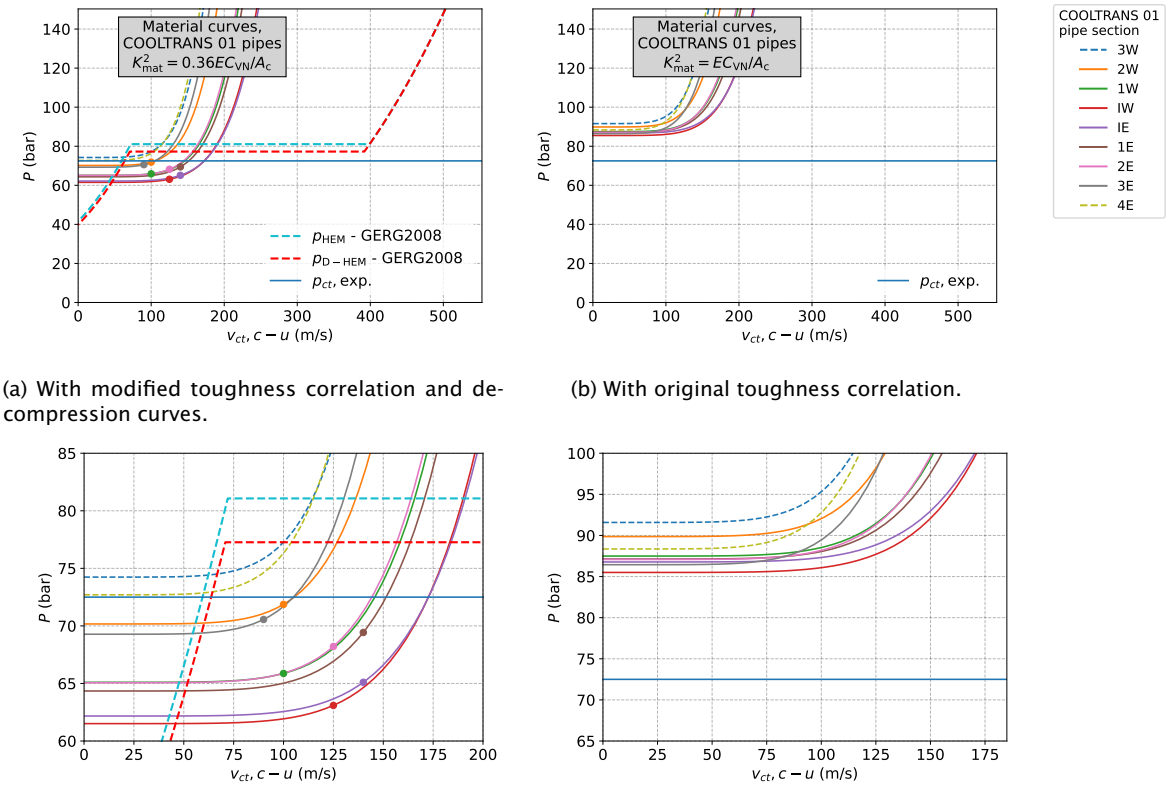

(a) With modified toughness correlation and decompression curves.

(b) With original toughness correlation.

(c) With modified toughness correlation and decompression curves (zoom-in).

(d) With original toughness correlation (zoom-in).

Figure 8: Two-curve plots for COOLTRANS Test 1 with and without updated toughness correlation. For the dashed material curves, arrest was observed experimentally. Fluid decompression curves for HEM and D-HEM are included in addition to the crack-tip pressure inferred from the experiment (Michal *et al.*, 2020).

same fluid mixture (see Table 2). COOLTRANS Test 2 similarly gave eight data points, with a different fluid mixture and initial condition. In Figure 8 and Figure 9 we have plotted the crack-tip pressure, P_{ct}, from Eq. (1) with $K_{\text{BF}} = 0.6 \times 10^{-3}\,\text{m}^2/\text{kg}^{0.5}$, for Test 1 and 2, respectively. Figures 8a and 9a show the result with the modified toughness correlation Eq. (9), and Figures 8b and 9b shows the results with the original correlation Eq. (4).

In the zoomed-in Figures 8c and 9c we also see the improved splitting of arrest and propagate data by our proposed method. The two propagate curves in Test 2 that do not intersect with the P_{ct} curve (2E and 2W) are the same propagate points that appear on the wrong side of the arrest correlation in Figures 4 and 5. The dots on the velocity curves are the observed velocities. Ideally, the velocities should have appeared at the intersection with P_{ct}. This is sensitive to uncertainties, both on the modelling side and the experimental side. E.g., a shift in P_{ct} of just a few bars can move the point of intersection 10–100 m/s. Here we have simply used the P_{ct} extracted by Michal *et al.* (2020), see Table 1.

From Figures 8b and 9b, we see that the original BTCM would predict 'arrest' in all pipe sections. The modified method in Figures 8a and 9a comes much closer to correctly separating 'arrest' from 'propagate'. Regarding the fluid curves (green (HEM), cyan (D-HEM), blue (experiment)), we observe that HEM yielded a plateau pressure about 8 bar above the experimentally observed crack-tip pressure for both tests. We also observe that D-HEM yielded a lower value; 4 bar above the experimental value for

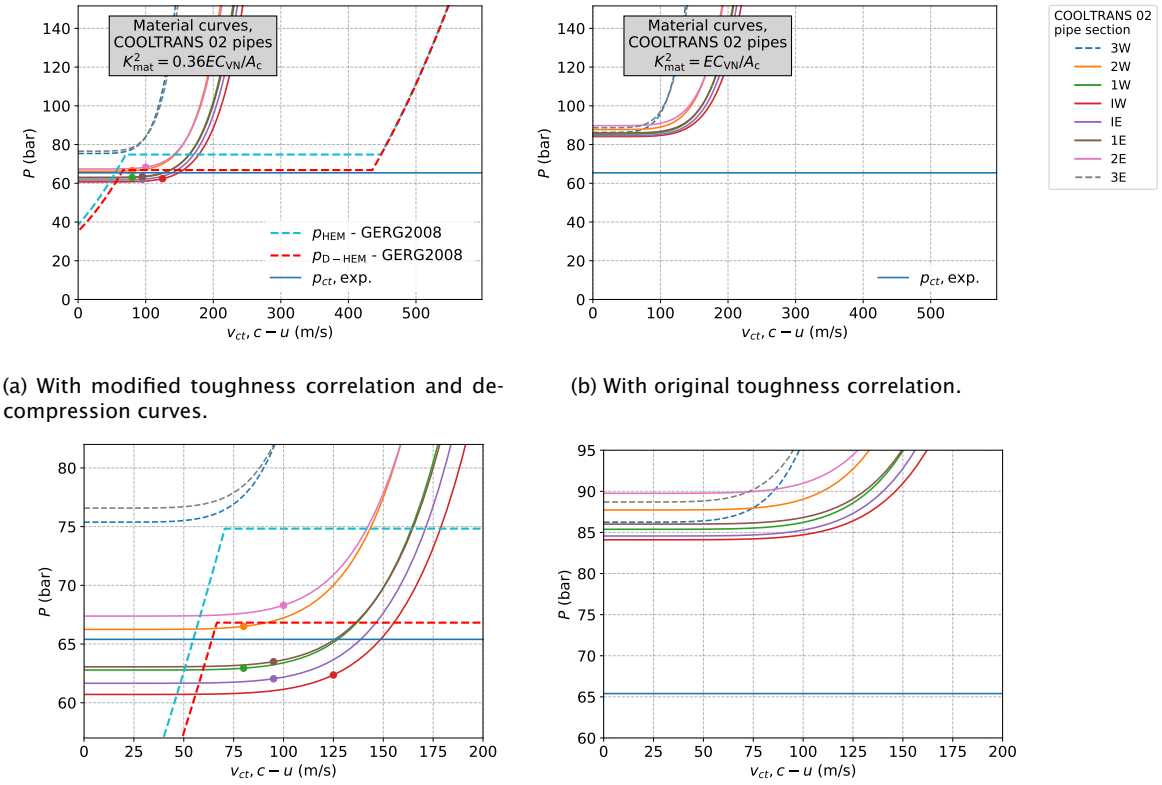

(a) With modified toughness correlation and decompression curves.

(b) With original toughness correlation.

(c) With modified toughness correlation and decompression curves (zoom-in).

(d) With original toughness correlation (zoom-in).

Figure 9: Two-curve plots for COOLTRANS Test 2 with and without updated toughness correlation. For the dashed material curves, arrest was observed experimentally. Fluid decompression curves for HEM and D-HEM are included in addition to the crack-tip pressure inferred from the experiment (Michal *et al.*, 2020).

Test 1 and 0.5 bar above the experimental value for Test 2. Given the uncertainties, we regard both results as very good.

Finally, we note that the results are highly sensitive to the crack-tip pressure. This means, e.g., that a small change in crack-tip pressure could move the crack arrest to a different pipe section.

4. Conclusion

The deployment of CCS as a climate change mitigation technology relies on establishing a massive CO_2 transportation system by the mid century, capable of transporting several gigatonnes per year. A large fraction of this CO_2 is expected to be transported in high-pressure pipelines. For the reuse of existing pipelines, or the design of new pipelines, it is vital to assess the design with respect to running ductile fracture.

For fluids such as natural gas, the Battelle two-curve method is the most commonly used engineering method for such assessments. In that method, the fracture-propagation speed in the steel and the decompression-wave speed in the fluid are drawn as a function of pressure level. It has been shown that the method is non-conservative for CO_2 pipelines. This, combined with the limited number of available full-scale fracture-propagation experiments, has led current practice to rely on special assessments.

In this work, we have suggested ways to modify the Battelle two-curve method for CO_2 pipelines. First, motivated by the different pressure distribution during fracture propagation, the material curve

was modified by changing the fracture toughness dependence on the Charpy V-notch value. Second, we have drawn the fluid curve using the D-HEM method, taking thermodynamic non-equilibrium into account. This gives a lower crack-tip pressure than the current common practice of employing the two-phase saturation pressure. The practical implication of this is two-fold, as it can avoid overdesign, and also the possible overestimation of material strength.

We have applied our method to the full-scale crack-propagation test data from COOLTRANS Tests 1 and 2 and obtained significantly improved predictions with respect to the original Battelle two-curve method. This indicates that our approach is viable and should be further developed. It also confirms that both fluid and material properties need to be correctly predicted when studying running ductile fracture.

We emphasize that more work is needed in order to arrive at an engineering method. In particular, the D-HEM method needs to be extended to a wider range of initial fluid conditions in order to cover heterogeneous nucleation.

Acknowledgement

This publication has been produced with support from the NCCS Research Centre, performed under the Norwegian research program Centres for Environment-friendly Energy Research (FME). The authors acknowledge the following partners for their contributions: Aker Carbon Capture, Allton, Ansaldo Energia, Baker Hughes, CoorsTek Membrane Sciences, Equinor, Fortum Oslo Varme, Gassco, Krohne, Larvik Shipping, Lundin Energy Norway, Norcem, Norwegian Oil and Gas, Quad Geometrics, Stratum Reservoir, TotalEnergies, Vår Energi, Wintershall Dea and the Research Council of Norway (257579).

References

Aasen, A., Reguera, D., Wilhelmsen, Ø., Jan 2020. Curvature corrections remove the inconsistencies of binary classical nucleation theory. *Phys. Rev. Lett.* 124, 045701. doi:10.1103/PhysRevLett.124.045701.

Aursand, E., Dumoulin, S., Hammer, M., Lange, H. I., Morin, A., Munkejord, S. T., Nordhagen, H. O., Sep. 2016a. Fracture propagation control in CO_2 pipelines: Validation of a coupled fluid-structure model. *Eng. Struct.* 123, 192–212. doi:10.1016/j.engstruct.2016.05.012.

Aursand, P., Gjennestad, M. A., Aursand, E., Hammer, M., Wilhelmsen, Ø., 2016b. The spinodal of single- and multi-component fluids and its role in the development of modern equations of state. *Fluid Phase Equilib.* 436, 98–112. doi:10.1016/j.fluid.2016.12.018.

Barták, J., Sep. 1990. A study of the rapid depressurization of hot water and the dynaics of vapour bubble generation in superheated water. *Int. J. Multiphase Flow* 16, 789–798. doi:10.1016/0301-9322(90)90004-3.

Benintendi, R., 2014. Non-equilibrium phenomena in carbon dioxide expansion. *Process Saf. Environ.* 92 (1), 47–59. doi:10.1016/j.psep.2013.11.001.

Bilio, M., Brown, S., Fairweather, M., Mahgerefteh, H., Nov. 2009. CO_2 pipelines material and safety considerations. In: *Hazards XXI*. vol. 155 of *Institution of Chemical Engineers Symposium Series*, pp. 423–429.

Borkar, G. S., Lienhard, J. H., Trela, M., 1977. *Rapid hot-water depressurization experiment*. Interim report, University of Kentucky Research Foundation. doi:10.2172/5053323.

Botros, K. K., Geerligs, J., Rothwell, B., Robinson, T., Jun. 2016. Measurements of decompression wave speed in pure carbon dioxide and comparison with predictions by equation of state. *J. Press. Vess. – T. ASME* 138 (3). doi:10.1115/1.4031941.

Cosham, A., Jones, D. G., Armstrong, K., Allason, D., Barnett, J., 24–28 Sep 2012. Ruptures in gas pipelines, liquid pipelines and dense phase carbon dioxide pipelines. In: *9th International Pipeline Conference, IPC2012*. ASME, IPTI, Calgary, Canada, vol. 3, pp. 465–482. doi:10.1115/IPC2012-90463.

Cosham, A., Jones, D. G., Armstrong, K., Allason, D., Barnett, J., 29 Sep–30 Oct 2014. Analysis of two dense phase carbon dioxide full-scale fracture propagation tests. In: *10th International Pipeline Conference, IPC2014*. Calgary, Canada. doi:10.1115/IPC2014-33080.

Cosham, A., Jones, D. G., Armstrong, K., Allason, D., Barnett, J., 26–30 Sep 2016. Analysis of a dense phase carbon dioxide full-scale fracture propagation test in 24 inch diameter pipe. In: *11th International Pipeline Conference, IPC2016*. American Society of Mechanical Engineers, Calgary, Canada. doi:10.1115/IPC2016-64456.

Cosham, A., Michal, G., Østby, E., Barnett, J., 26–30 Sep 2022. The decompressed stress level in dense phase carbon dioxide full-scale fracture propagation tests. In: *14th International Pipeline Conference, IPC2022*. ASME, IPTI, Calgary, Canada, vol. 3. doi:10.1115/IPC2022-86855.

d'Amore, F., Mocellin, P., Vianello, C., Maschio, G., Bezzo, F., Aug. 2018. Economic optimisation of European supply chains for CO_2 capture, transport and sequestration, including societal risk analysis and risk mitigation measures. *Appl. Energ.* 223, 401–415. doi:10.1016/j.apenergy.2018.04.043.

Debenedetti, P. G., 1997. *Metastable Liquids: Concepts and Principles*. Princeton University Press. ISBN 9780691213941. doi:10.1515/9780691213941.

Di Biagio, M., Lucci, A., Mecozzi, E., Spinelli, C. M., May 2017. Fracture propagation prevention on CO_2 pipelines: Full scale experimental testing and verification approach. In: *12th Pipeline Technology Conference*. Lab. Soete and Tiratsoo Technical, Berlin, Germany. Paper no. S06-02.

DNV, Aug. 2012. Submarine pipeline systems. Offshore standard DNV-OS-F-101.

DNVGL, Feb. 2021. Design and operation of carbon dioxide pipelines. Recommended practice DNVGL-RP-F104.

Edenhofer, O., Pichs-Madruga, R., Sokona, Y., Farahani, E., Kadner, S., Seyboth, K., Adler, A., Baum, I., Brunner, S., Eickemeier, P., Kriemann, B., Savolainen, J., Schlømer, S., von Stechow, C., Zwickel, T., (eds.), J. M., 2014. *Climate Change 2014: Mitigation of Climate Change*. Tech. rep., Working Group III Contribution to the Fifth Assessment Report of the Intergovernmental Panel on Climate Change, Summary for Policymakers, IPCC. URL http://mitigation2014.org/.

Flechas, T., Laboureur, D. M., Glover, J., Charles, Aug. 2020. A 2-D CFD model for the decompression of carbon dioxide pipelines using the Peng-Robinson and the Span-Wagner equation of state. *Process Saf. Environ.* 140, 299–313. doi:10.1016/j.psep.2020.04.033.

Folias, E. S., 1970. On the theory of fracture of curved sheets. *Eng. Fract. Mech.* 2 (2), 151–164. doi:10.1016/0013-7944(70)90019-6.

Gruben, G., Dumoulin, S., Nordhagen, H., Hammer, M., Munkejord, S. T., Jun. 2019. Calibration of pipeline steel model for computational running ductile fracture assessment. In: *ISOPE 2019 – 29th International Ocean and Polar Engineering Conference*. Honolulu, Hawaii, USA. Paper ISOPE-I-19-347.

Gu, S., Li, Y., Teng, L., Hu, Q., Zhang, D., Ye, X., Wang, C., Wang, J., Iglauer, S., 2018. A new model for predicting the decompression behavior of CO_2 mixtures in various phases. *Process Saf. Environ.* 120, 237–247. doi:10.1016/j.psep.2018.08.034.

Gu, S., Li, Y., Teng, L., Wang, C., Hu, Q., Zhang, D., Ye, X., Wang, J., Iglauer, S., May 2019. An experimental study on the flow characteristics during the leakage of high pressure CO_2 pipelines. *Process Saf. Environ.* 125, 92–101. doi:10.1016/j.psep.2019.03.010.

Hammer, M., Aasen, A., Wilhelmsen, Ø., 2020. Thermopack. https://github.com/SINTEF/thermopack/. Accessed 2020-12-15.

Hammer, M., Deng, H., Austegard, A., Log, A. M., Munkejord, S. T., Nov. 2022. Experiments and modelling of choked flow of CO_2 in orifices and nozzles. *Int. J. Multiphase Flow* 156, 104201. doi:10.1016/j.ijmultiphaseflow.2022.104201.

Huber, M. L., Lemmon, E. W., Bell, I. H., McLinden, M. O., Jun. 2022. The NIST REFPROP database for highly accurate properties of industrially important fluids. *Ind. Eng. Chem. Res.* doi:10.1021/acs.iecr.2c01427.

IEA, 2021. *Net Zero by 2050 – A Roadmap for the Global Energy Sector*. IEA, Paris. doi:10.1787/c8328405-en. URL https://www.iea.org/reports/net-zero-by-2050.

ISO, Nov. 2016. Carbon dioxide capture, transportation and geological storage – pipeline transportation systems. Standard 27913.

Ives, K. D., Shoemaker, A. K., McCartney, R. F., Oct. 1974. Pipe deformation during a running shear fracture in line pipe. *J. Eng. Mater. – T. ASME* 96 (4), 309–317. doi:10.1115/1.3443246.

Keim, V., Marx, P., Nonn, A., Münstermann, S., Aug. 2019. Fluid-structure-interaction modeling of dynamic fracture propagation in pipelines transporting natural gases and CO_2-mixtures. *Int. J. Pres. Ves. Pip.* 175, 103934. doi:10.1016/j.ijpvp.2019.103934.

Keim, V., Paredes, M., Nonn, A., Münstermann, S., May 2020. FSI-simulation of ductile fracture propagation and arrest in pipelines: Comparison with existing data of full-scale burst tests. *Int. J. Pres. Ves. Pip.* 182, 104067. doi:10.1016/j.ijpvp.2020.104067.

Kiefner, J. F., Maxey, W. A., Eiber, R. J., Duffy, A. R., 1973. Failure stress levels of flaws in pressurized cylinders. In: Kaufman, J. G. (Ed.), *Progress in flaw growth and fracture toughness testing*, American Society for Testing and Materials, vol. 536 of *ASTM Special Technical Publication*, pp. 461–481. doi:10.1520/STP49657S.

Kunz, O., Wagner, W., October 2012. The GERG-2008 wide-range equation of state for natural gases and other mixtures: An expansion of GERG-2004. *J. Chem. Eng. Data* 57 (11), 3032–3091. doi:10.1021/je300655b.

Leis, B. N., Eiber, R. J., Carlson, L., Gilroy-Scott, A., Jun. 1998. Relationship between apparent (total) Charpy vee-notch toughness and the corresponding dynamic crack-propagation resistance. In: *2nd International Pipeline Conference, IPC1998*. ASME, Calgary, Canada, vol. 2. doi:10.1115/ipc1998-2084.

Lienhard, J. H., Alamgir, M., Trela, M., Aug. 1978. Early response of hot water to sudden release from high pressure. *J. Heat Transfer* 100 (3), 473–479. doi:10.1115/1.3450833.

Linga, G., Flåtten, T., Sep. 2019. A hierarchy of non-equilibrium two-phase flow models. *ESAIM: Proceedings and Surveys* 66, 109–143. doi:10.1051/proc/201966006.

Lopes, J. T., Francesconi, A. Z., Vianna, S. S. V., Jan. 2018. Modelling of source term from accidental release of pressurised CO_2. *Process Saf. Environ.* 113, 88–96. doi:10.1016/j.psep.2017.08.046.

Martynov, S., Brown, S., Mahgerefteh, H., Sundara, V., Chen, S., Zhang, Y., 2014. Modelling three-phase releases of carbon dioxide from high-pressure pipelines. *Process Saf. Environ.* 92 (1), 36–46. doi:10.1016/j.psep.2013.10.004.

Maxey, W. A., Nov. 1974. Fracture initiation, propagation and arrest. In: *Fifth Symposium on Line Pipe Research*. American Gas Association, Houston, Texas, USA, pp. J1–J31.

Maxey, W. A., Aug. 1986. Long shear fractures in CO_2 lines controlled by regulating saturation, arrest pressures. *Oil Gas J.* 84 (31), 44–46.

Maxey, W. A., Kiefner, J. F., Eiber, R. J., Duffy, A. R., 1972. Ductile fracture initiation, propagation, and arrest in cylindrical vessels. In: *Fracture Toughness: Part II*, ASTM International. doi:10.1520/stp38819s.

Michal, G., Davis, B., Østby, E., Lu, C., Røneid, S., 2018. CO2SAFE-ARREST: A full-scale burst test research program for carbon dioxide pipelines – Part 2: Is the BTCM out of touch with dense-phase co2? In: *12th International Pipeline Conference, IPC*

2018. ASME. doi:10.1115/IPC2018-78525.
Michal, G., Østby, E., Davis, B. J., Røneid, S., Lu, C., Sep. 2020. An empirical fracture control model for dense-phase CO2 carrying pipelines. In: *13th International Pipeline Conference, IPC 2020*. ASME. doi:10.1115/IPC2020-9421.
Morland, B. H., Dugstad, A., Svenningsen, G., sep 2022. Experimental based CO_2 transport specification ensuring material integrity. *Int. J. Greenh. Gas Con.* 119, 103697. doi:10.1016/j.ijggc.2022.103697.
Munkejord, S. T., Austegard, A., Deng, H., Hammer, M., Stang, H. G. J., Løvseth, S. W., Nov. 2020. Depressurization of CO_2 in a pipe: High-resolution pressure and temperature data and comparison with model predictions. *Energy* 211, 118560. doi:10.1016/j.energy.2020.118560.
Munkejord, S. T., Deng, H., Austegard, A., Hammer, M., Skarsvåg, H. L., Aasen, A., Jul. 2021. Depressurization of CO_2-N_2 and CO_2-He in a pipe: Experiments and modelling of pressure and temperature dynamics. *Int. J. Greenh. Gas Con.* 109, 103361. doi:10.1016/j.ijggc.2021.103361.
Munkejord, S. T., Hammer, M., Løvseth, S. W., May 2016. CO_2 transport: Data and models – A review. *Appl. Energ.* 169, 499–523. doi:10.1016/j.apenergy.2016.01.100.
Nakai, H., Shibanuma, K., Aihara, S., Aug. 2016. Numerical model for unstable ductile crack propagation and arrest in pipelines using finite difference method. *Eng. Fract. Mech.* 162, 179–195. doi:10.1016/j.engfracmech.2016.03.048.
Nordhagen, H. O., Munkejord, S. T., Hammer, M., Gruben, G., Fourmeau, M., Dumoulin, S., Jul. 2017. A fracture-propagation-control model for pipelines transporting CO_2-rich mixtures including a new method for material-model calibration. *Eng. Struct.* 143, 245–260. doi:10.1016/j.engstruct.2017.04.015.
Pham, L. H. H. P., Rusli, R., 2016. A review of experimental and modelling methods for accidental release behaviour of high-pressurised CO_2 pipelines at atmospheric environment. *Process Saf. Environ.* 104, 48–84. doi:10.1016/j.psep.2016.08.013.
Schenk, M. R., Köddermann, T., Kirschner, K. N., Knauer, S., Reith, D., 2020. Molecular dynamics in the energy sector: Experiment and modeling of the CO_2/CH_4 mixture. *J. Chem. Eng. Data* 65, 1117–1123. doi:10.1021/acs.jced.9b00503.
Talemi, R. H., Cooreman, S., Mahgerefteh, H., Martynov, S., Brown, S., Jun. 2019. A fully coupled fluid-structure interaction simulation of three-dimensional dynamic ductile fracture in a steel pipeline. *Theor. Appl. Fract. Mec.* 101, 224–235. doi:10.1016/j.tafmec.2019.02.005.
Teng, L., Liu, X., Li, Y., Lu, C., Oct. 2021. An approach of quantitative risk assessment for release of supercritical CO_2 pipelines. *J. Nat. Gas Sci. Eng.* 94, 104131. doi:10.1016/j.jngse.2021.104131.
Vitali, M., Corvaro, F., Marchetti, B., Terenzi, A., 2022. Thermodynamic challenges for CO_2 pipelines design: A critical review on the effects of impurities, water content, and low temperature. *Int. J. Greenh. Gas Con.* 114, 103605. doi:10.1016/j.ijggc.2022.103605.
Wilhelmsen, Ø., Aasen, A., 2022. Choked liquid flow in nozzles: Crossover from heterogeneous to homogeneous cavitation and insensitivity to depressurization rate. *Chem. Eng. Sci.* 248, 117176. doi:10.1016/j.ces.2021.117176.
Wilhelmsen, Ø., Aasen, A., Skaugen, G., Aursand, P., Austegard, A., Aursand, E., Gjennestad, M. A., Lund, H., Linga, G., Hammer, M., 2017. Thermodynamic modeling with equations of state: Present challenges with established methods. *Ind. Eng. Chem. Res.* 56 (13), 3503–3515. doi:10.1021/acs.iecr.7b00317.
Wilkowski, G., Wang, Y. Y., Rudland, D., 2000. Recent efforts on characterizing propagating ductile fracture resistance of linepipe steels. In: *Proceedings of the 3rd Pipeline Technology Conference*. pp. 359–386.
Wilkowski, G. M., Maxey, W. A., Eiber, R. J., 1977. Use of a brittle notch DWTT specimen to predict fracture characteristics of line pipe steels. In: *ASME 1977 Energy Technology Conference, Houston, Texas*. pp. 18–22.
Zhao, Q., Li, Y.-X., Jan. 2014. The influence of impurities on the transportation safety of an anthropogenic CO_2 pipeline. *Process Saf. Environ.* 92 (1), 80–92. doi:10.1016/j.psep.2013.10.007.

Nomenclature

Latin letters

A	Charpy specimen cross-section area	m^2
a_c	Half-length of through-wall flaw	m
c	Speed of sound	m/s
C_{VN}	Charpy V-notch value	J
E	Young's modulus	Pa
G	Bubble work of formation	J
h	Enthalpy	J/kg
J	Nucleation rate	$1/(m^3\,s)$
k_B	Boltzmann constant	J/K
K	Kinetic prefactor	$1/(m^3\,s)$
K_{BF}	Backfill parameter	$kg^2\,m^{0.5}$
K_{mat}	Fracture resistance parameter	J^2/m^4
m	Mass of one molecule	kg
M_T	Folias factor	1
$\tilde{N}$	Total number density	$1/m^3$

P	Pressure	Pa
R	Pipe outer radius	m
r	Radius	m
R_f	Fracture resistance parameter	1
R_σ	Stress-ratio parameter	1
T	Temperature	K
t	Pipe wall thickness	m
u	Fluid velocity	m/s
V	Volume	m^3
v	Velocity	m/s
Y	Vapour molar fraction	mol/mol

Greek letters

ε	Relative difference	%
ρ	Mass density	kg/m^3
$\bar{\sigma}$	Flow stress	Pa
σ	Surface tension	N/m

Subscripts

0	Initial
a	Arrest
bub	Bubble point
choke	Choke
C	Component
cr	Critical
ct	Crack tip
eq	Equilibrium
exp	Experiment
f	Fracture
ℓ	Liquid
sat	Saturation
tot	Total

Superscripts

$*$	Critically-sized
$'$	Integrated quantity
eff	Effective
W	Wilkowski

Abbreviations

BTCM	Battelle two-curve method
CCS	CO_2 Capture and storage
CFD	Computational fluid dynamics
CNT	Classical nucleation theory
D-HEM	Delayed homogeneous equilibrium model
EoS	Equation of state
FEM	Finite-element method
HEM	Homogeneous equilibrium model
NG	Natural gas
RDF	Running ductile fracture
SHL	Superheat limit
SI	International System of Units

Appendix A. Assessment of the accuracy of the REFPROP parachor method

In the delayed homogeneous equilibrium model (D-HEM) method for mixtures, we employ the REFPROP (Huber *et al.*, 2022) parachor method to estimate mixture surface tension. The accuracy of the method is not documented. In order to quantify this some extent for CO_2-mixtures, we compare model predictions to measured surface tensions of a CO_2-CH_4 mixture (Schenk *et al.*, 2020). The relative difference was computed as follows:

$$\varepsilon = \frac{\sigma_{\text{REFPROP}} - \sigma_{\text{exp}}}{\sigma_{\text{exp}}} \cdot 100\%. \tag{A.1}$$

Some of the experimental measurements reported by Schenk *et al.* (2020) have quite large uncertainty. We therefore report whether the relative difference between the REFPROP estimate and the experiment is within the experimental uncertainty. The results are summarized in Table A.3. For five out of seven experimental points, the model predictions match the experiments within the uncertainty. Therefore we conclude that the parachor method can be expected to yield reasonable results for CO_2-rich mixtures.

Appendix B. Effect of the superheat limit

Appendix B.1. Calculation of the superheat limit

The superheat limit (SHL) can be estimated using classical nucleation theory. This is done by correlating the SHL to the rate of nucleation of bubbles large enough to grow as predicted by CNT. Such bubbles are just large enough not to collapse back into the liquid, and are called *critically-sized*. In the following, the properties of these bubbles are denoted by an asterisk, $*$. As described by Debenedetti (1997), the rate of nucleation of such bubbles per volume and time can be expressed as

$$J = K \exp\left(-\frac{\Delta G^*}{k_B T_\ell}\right), \tag{B.1}$$

where ΔG is the free-energy barrier of bubble formation, k_B is the Boltzmann constant and K is a kinetic prefactor. The free-energy barrier is estimated to be

$$\Delta G^* = \frac{4\pi\sigma r^{*2}}{3}, \tag{B.2}$$

where σ denotes the surface tension and r the radius of the bubble. It is assumed that the surface tension of the bubble, σ, is equal to the macroscopic surface tension of a planar interface between the phases at the bubble curve. In the present work, the mixture surface tension is approximated using the parachor method applied in REFPROPv10 (Huber *et al.*, 2022). A main advantage of the parachor method is that the surface tension goes to zero at the critical point of the mixture. This provides consistent results near the critical point, where the energy barrier of bubble formation should vanish.

Table A.3: Comparison of the mixture surface tension measured experimentally (Schenk *et al.*, 2020) and estimated by the REFPROP parachor method (Huber *et al.*, 2022) for a CO_2-CH_4 mixture.

T (°C)	P (bar)	σ_{exp} (mN/m)	σ_{REFPROP} (mN/m)	ε (%)	Within exp. uncertainty?
−50	30	8.7 ± 1.0	9.5	9.2	yes
−50	39	6.0 ± 0.4	7.2	20.0	no
−50	55	3.0 ± 0.7	2.8	−6.7	yes
−40	30	9.4 ± 1.1	8.5	−9.6	yes
−40	41	6.1 ± 0.7	6.2	1.6	yes
−40	50	4.6 ± 0.5	4.3	−6.5	yes
−40	51	3.6 ± 0.1	4.1	13.9	no

Table B.4: Sensitivity of the superheat-limit pressure, P_{SHL}, in the D-HEM approach for the different CO_2-mixture RDF tests for different choices of critical nucleation rate, J_{cr}. The crack-tip pressure, P_{ct}, evaluated by Michal *et al.* (2020) is also provided for reference.

	P_{SHL} (bar)				P_{ct} (bar)
Test	$J_{cr} = 10^{6}\,1/(m^3\,s)$	$J_{cr} = 10^{12}\,1/(m^3\,s)$	$J_{cr} = 10^{18}\,1/(m^3\,s)$	$J_{cr} = 10^{24}\,1/(m^3\,s)$	
COOLTRANS-1	77.5	77.1	76.6	75.7	73.5
COOLTRANS-2	67.6	66.8	65.7	63.8	66.4
COOLTRANS-3	88.2	88.0	87.7	87.2	82
SARCO2-B	70.4	70.0	69.6	66.9	68
CO2SAFE-ARREST 1	76.4	76.1	75.6	74.8	65
CO2SAFE-ARREST 2	83.2	83.0	82.7	82.3	74.5

The threshold radius for bubble formation is approximated as

$$r^* = \frac{2\sigma}{P_{bub}(T_\ell) - P_\ell}, \tag{B.3}$$

where $P_{bub}(T_\ell)$ is the bubble curve pressure at the liquid temperature. Debenedetti (1997) states that results for mixtures are in many cases well-correlated by approximating the kinetic prefactor as

$$K = \tilde{N}_{tot}\sqrt{\frac{2\sigma}{\pi}}m^{1/2}, \tag{B.4}$$

where the total number density, $\tilde{N}_{tot}$, is written as the sum of component number densities in the liquid:

$$\tilde{N}_{tot} = \sum_{i=1}^{N_C}\frac{\rho_{i,\ell}}{m_i}. \tag{B.5}$$

Here, N_C is the number of components in the liquid and m_i is the mass of one molecule of component i. Furthermore, $m^{1/2}$ can be approximated by

$$m^{1/2} = \sum_{i=1}^{N_C}\frac{Y_i}{\sqrt{m_i}}, \tag{B.6}$$

where Y_i is component i's vapour-phase mole fraction at $T = T_\ell$, $P = P_{bub}(T_\ell)$.

The SHL temperature can be estimated by solving

$$J(T_\ell) = J_{cr} \tag{B.7}$$

for T_ℓ. Here, J_{cr} is the critical nucleation rate, at which sudden phase change is observed (Aursand *et al.*, 2016b). In this work, we follow Aursand *et al.* (2016b), employing $J_{cr} = 1 \times 10^{12}/(m^3\,s)$.

Appendix B.2. Sensitivity of the superheat limit and the superheat-limit pressure, P_{SHL}

The effect of different choices of the critical rate on the SHL is shown in Figure B.10a for the mixture studied in COOLTRANS Test 2 (Cosham *et al.*, 2016). The effect is limited even for a variation of ± six orders of magnitude. As the critical temperature is approached, the effect diminishes. At $T = -10\,°C$, the difference in the SHL pressures for the different J_{cr}s is approximately ±2 bar. Table B.4 shows the superheat-limit pressure, P_{SHL}, calculated using the D-HEM method for varying critical nucleation rate, J_{cr}. It can be seen that the sensitivity is low, even for a huge span in J_{cr}.

In addition to the critical nucleation rate, J_{cr}, the surface tension, σ, is a key parameter in determining the SHL. No data are available to assess the accuracy of the parachor surface tension model for the

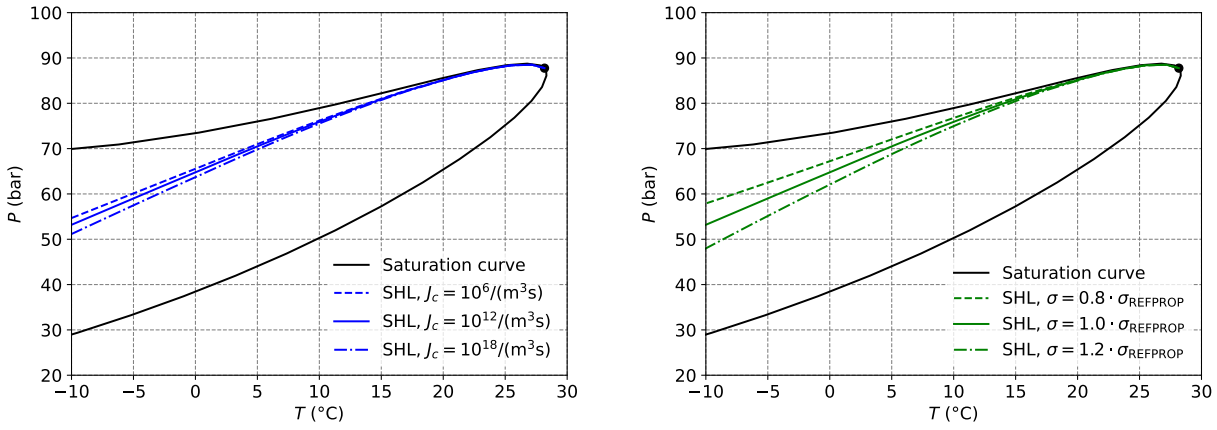

Figure B.10: The effect on the estimated superheat limit (SHL) when varying the critical nucleation rate J_{cr} (a) and the surface tension σ (b). The critical point is marked as a black dot.

Table B.5: Sensitivity of the superheat-limit pressure, P_{SHL}, in the D-HEM approach for the different CO_2-mixture RDF tests due to a ±20 % variation in the surface tension estimate. The crack-tip pressure, P_{ct}, evaluated by Michal *et al.* (2020) is also provided for reference.

	P_{SHL} (bar)			P_{ct} (bar)
Test	$\sigma = 0.8 \cdot \sigma_{REFPROP}$	$\sigma = \sigma_{REFPROP}$	$\sigma = 1.2 \cdot \sigma_{REFPROP}$	
COOLTRANS-1	78.3	77.1	75.8	73.5
COOLTRANS-2	69.2	66.8	64.0	66.4
COOLTRANS-3	88.6	88.0	87.3	82
SARCO2-B	71.0	70.0	69.0	68
CO2SAFE-ARREST 1	77.1	76.1	74.9	65
CO2SAFE-ARREST 2	83.6	83.0	82.4	74.5

mixtures in the various RDF tests considered here (Cosham *et al.*, 2014, 2016; Di Biagio *et al.*, 2017; Michal *et al.*, 2018). To find an estimate of the accuracy of the parachor method, the results of the method were compared to experimental measurements of the surface tension for a CO_2-CH_4 mixture conducted by Schenk *et al.* (2020). The relative deviations for the six data points are presented in Table A.3 and the largest relative deviation was 20 %. In the following discussion, we therefore make the assumption that the uncertainty is ±20 %.

In Figure B.10b, we show the effect of a 20 % error in the surface tension on the predicted SHL for COOLTRANS Test 2 (Cosham *et al.*, 2016). As can be seen, the effect is largest at cold temperatures. At $T = -10\,°C$, the difference in the SHL pressure for a 20 % offset in σ is approximately ±5 bar.

Increasing or decreasing the surface tension will affect where the superheat limit lies in the temperature-pressure space. The liquid isentrope will therefore cross the superheat limit at different pressures, P_{SHL}, giving different plateau pressures in the D-HEM method for calculating the fluid decompression curve in BTCM. A summary of the variation in P_{SHL} for the different CO_2-mixture RDF tests due to a ±20 % variation in the surface tension estimate is provided in Table B.5. The largest sensitivity due to a ±20 % variation in the surface tension is for the COOLTRANS-2 test. Here, the difference in P_{SHL} is approximately ±2.8 bar. The sensitivity increases for tests conducted at lower temperatures, i.e., further away from the critical temperature.